Edge states of zigzag bilayer graphite nanoribbons

2008 J. Phys.: Condens. Matter 20 365202

(http://iopscience.iop.org/0953-8984/20/36/365202)

IOP PUBLISHING JOURNAL OF PHYSICS: CONDENSED MATTER

J. Phys.: Condens. Matter **20** (2008) 365202 (8pp) doi:10.1088/0953-8984/20/36/365202

Edge states of zigzag bilayer graphite nanoribbons

Jun-Won Rhim and Kyungsun Moon

Department of Physics and Institute of Physics and Applied Physics, Yonsei University, Seoul 120-749, Korea

E-mail: kmoon@yonsei.ac.kr

Received 15 May 2008, in final form 22 July 2008
Published 12 August 2008
Online at stacks.iop.org/JPhysCM/20/365202

Abstract

The electronic structures of zigzag bilayer graphite nanoribbons (Z-BGNRs) with various ribbon widths N are studied within the tight binding approximation. Neglecting the inter-layer hopping amplitude γ_4, which is an order of magnitude smaller than the other inter-layer hopping parameters, there exist two fixed Fermi points $\pm k^*$ independent of the ribbon width with a peculiar energy dispersion near k^* as $\varepsilon(k) \sim \pm(k - k^*)^N$. By investigating the edge states of Z-BGNRs, we notice that the trigonal warping of the bilayer graphene sheets is reflected in the edge state structure. With the inclusion of γ_4, the above two Fermi points are not fixed but drift toward the vicinity of the Dirac point with increasing width N, as shown by the finite scaling method, and the peculiar dispersions change to parabolic ones. The edge magnetism of Z-BGNRs is also examined by solving the half-filled Hubbard Hamiltonian for the ribbon using the Hartree–Fock approximation. We have shown that within the same side of the edges, the edge spins are aligned ferromagnetically for the experimentally relevant set of parameters.

(Some figures in this article are in colour only in the electronic version)

1. Introduction

Graphite nanoribbons (GNRs) are quasi-one-dimensional carbon sheets whose width and chirality can be well controlled by current nano-lithography techniques [1]. Due to the high mobility of the sample and the relativistic energy dispersion relation of the massless Dirac fermion, there has been a lot of interest both theoretically and experimentally in investigating the electronic properties of GNRs [2–17]. The electronic properties of GNRs are closely controlled by their chirality, as is well known for the case of carbon nanotubes. Among the GNRs with different chiralities, armchair and zigzag GNRs have been studied most intensively [2–6, 9–17]. Unlike carbon nanotubes with a compact angle that varies for transverse modes, a GNR can support edge states. Recently, the edge states of zigzag GNRs have been of great interest due to their peculiar dispersion relation with almost flat edge bands near zero energy [3, 14, 15]. When Coulomb interactions are taken into account, the existence of flat edge bands may lead to edge magnetism for various kinds of ribbon edges [3, 17–19]. It has been shown that the edge magnetism of zigzag GNRs is ferromagnetic along each edge and anti-ferromagnetic between the two different edges due to the bipartite nature of the lattice structure. This kind of edge magnetism has been widely studied within first-principles calculations [20–23]. Furthermore, its potential as a half-metallic material under a lateral electric field has been demonstrated within a first-principles approach by Son *et al* [18]. Hence, to identify the edge states of the various GNRs it is crucial to understand both the magnetic and electric properties of the system.

In the paper we study the electronic and magnetic structure of a zigzag bilayer GNR with various ribbon widths N. First, we give a brief review of the bilayer graphene system. The bilayer graphene system consists of two coupled graphene sheets and its tight binding electronic structures are determined by four leading characteristic hopping parameters, as shown in figure 1(a). This system has demonstrated quite unique electronic properties compared to a single graphene sheet, such as a larger Hall step and different kinds of chiral quasiparticles and distinct electronic structures [24]. The most distinctive electronic feature of the bilayer graphene system is the existence of trigonal warping of the Fermi level in the vicinity of the Dirac points, as demonstrated in the inset of figure 2(a). This means that the band of the graphite bilayer near the Dirac point does not form a cone but a trigonally curved cone and there are three additional pockets along

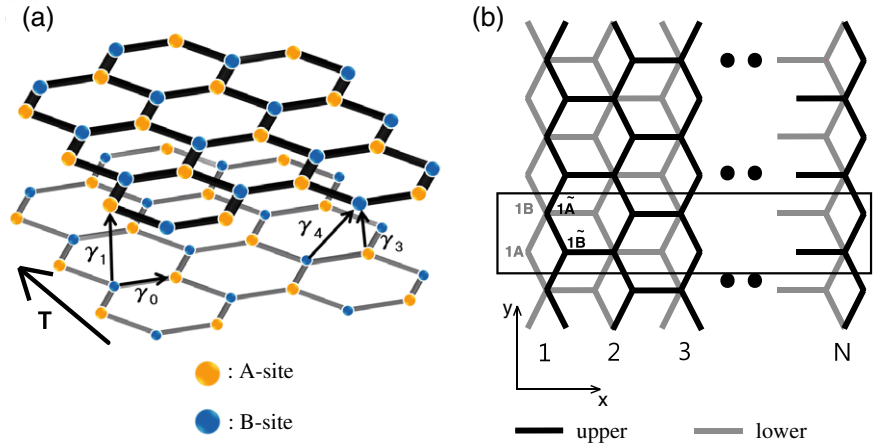

Figure 1. (a) Our model system of Bernal stacked Z-BGNR. Both the three inter-layer (γ_1, γ_3 and γ_4) and one intra-layer hopping (γ_0) parameters are shown. The Z-BGNR has a translational symmetry along $\vec{T}$. The sublattice A is colored yellow (pale gray) while B is colored green (dark gray). (b) Definition of the width of the Z-BGNR. Here the red lines (pale gray) are the lower graphene sheet and the black lines the upper one. The tildes above A and B stand for the upper layer and the black box represents a unit cell of the Z-BGNR.

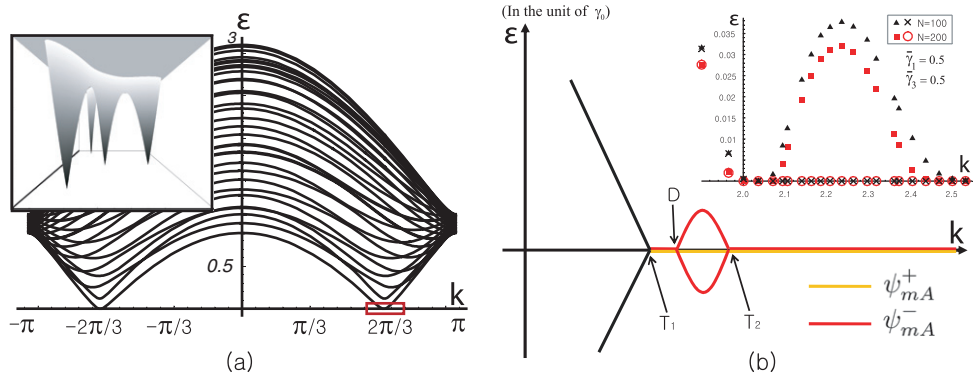

Figure 2. (a) Projected band structure of the 2D graphite bilayer along the direction of the zigzag axis. The boxed region near the Dirac point is magnified in the inset, which shows trigonal warping. D is the Dirac point at $k = 2\pi/3$ and three L points are the Fermi points of three nearby pockets. (b) A schematic diagram of the zero-energy edge states of a semi-infinite Z-BGNR near the Dirac point within the red box in (a). At $\varepsilon = 0$, the two eigenstates are drawn with different colors. Red (dark gray) for ψ_- and yellow (pale gray) for ψ_+. D is the Dirac point while T_1, T_2, and the two warped bands reflect the effect of trigonal warping of the graphite bilayer. The inset shows the energy dispersion curve obtained by a numerical method for Z-BGNRs with finite widths $N = 100, 200$.

the directions of zigzag chirality. It has been shown that these peculiar electronic structures, which are controlled by the inter-layer hopping parameters γ_1 and γ_3, produce extra degeneracies in the Landau levels. The three extra Dirac cones are known to play an important role in determining the minimal conductivity of the graphite bilayer [25].

In this work we focus on the edge state structure of Z-BGNRs with various ribbon widths N. Since the three legs in the band structure of the graphite bilayer lie along the direction of zigzag chirality, we have chosen Z-BGNRs in order to see the possible signature of trigonal warping imprinted on the edge state structure of the system. The schematic structure of a Z-BGNR is shown in figure 1(a). We have chosen Bernal stacked GNRs, where the widths of the two layers are the same and the width is defined to be the number of dimer lines N, as shown in figure 1(b). We use the tight binding method to calculate the band structures of Z-BGNRs with varying widths. According to the experimental data, the inter-layer hopping amplitude γ_4 is much smaller than γ_3 by an order of magnitude [26]. Neglecting γ_4, we notice that the Z-BGNR has two fixed Fermi points at $k = \pm k^*$ with $k^* = 2\cos^{-1}(\sqrt{\tilde{\gamma}_1\tilde{\gamma}_3}/2)$ and the following energy dispersion relation $\varepsilon \sim \pm(k - k^*)^N$. As N goes to infinity, a dispersionless edge band appears. By analyzing the semi-infinite Z-BGNR case analytically, we have demonstrated that trigonal warping manifests itself in the edge band structure of a Z-BGNR. Interestingly, the existence of the edge states seems to be consistent with the condition imposed by the Berry phase argument [27]. With the inclusion of γ_4, the particle–hole symmetry is broken and the energy gap appears in the dispersion. In this case, the conduction band minimum and the valence band maximum occur at two different points, k^{e} and k^{h}, respectively. They are no longer fixed points independent of N but rather drift toward the Dirac point with increasing N. By examining a semi-infinite Z-BGNR with γ_4 taken perturbatively and using the scaling method as well,

we have analyzed the edge states in further detail. We notice that one edge band remains flat while the other edge band becomes dispersive. These two edge bands appear below $\varepsilon = 0$ and split in proportion to the hopping parameter γ_4. Finally, the magnetic properties of Z-BGNRs are studied by investigating the Hubbard Hamiltonian obtained from the inclusion of the on-site Coulomb repulsion U based on the Hartree–Fock approximation. We have calculated the magnetic moments at the edge as a function of U for a half-filled system at zero temperature. Our main concern is that the possible half-metallicity would persist in a Z-BGNR upon lateral gate bias. Our result has shown that for a realistic value of U ($U/\gamma_0 \cong 1$), the ferromagnetic alignment of the edge spins within the same side of the edges is favorable. This implies that spintronic application of Z-BGNRs is quite promising.

The paper is organized as follows. In section 2, a detailed description of the tight binding model for Z-BGNRs is given. In section 3, we investigate the electronic structures of Z-BGNRs with or without the small inter-layer hopping parameter γ_4. We focus on the edge state structure based on the formulae of section 2. Without γ_4, the coupled equation to obtain the energy dispersion relation can be simplified and one can extract the important features of the edge states in the system. We analyze the semi-infinite Z-BGNRs to obtain the analytic formulae of the edge state amplitudes. In section 4, the inter-layer edge magnetism of a Z-BGNR is studied by including the Hubbard type onsite interactions. Finally, summaries will be given in section 5.

2. Tight binding Hamiltonian

We introduce the tight binding model for Z-BGNRs by considering the four hopping parameters $\gamma_0, \gamma_1, \gamma_3$ and γ_4, where γ_0 is the intra-layer hopping and the others are inter-layer hopping amplitudes as shown in figure 1(a). This type of approach has been successfully employed in the study the electronic structure due to the p_z-orbital of various carbon based materials including GNRs [3, 15, 16]. We begin with the following Hamiltonian:

$$H = -\sum_{\langle i,j\rangle} t_{ij} c_i^\dagger c_j \tag{1}$$

with

$$t_{ij} = \langle \varphi(\vec{r} - \vec{R}_i)|H|\varphi(\vec{r} - \vec{R}_j)\rangle \tag{2}$$

where the summations over i and j include all the hopping processes related to the four hopping parameters. For the sake of simplicity, we redefine the index i in terms of the following three indices such as $c_i = c_\alpha(m, \lambda)$, where α represents the unit cell of a Z-BGNR, m is the index of dimer lines which runs from 1 to N, and λ one of the four sublattices $A, B, \tilde{A}$ and $\tilde{B}$ as shown in figure 1(b). By transforming this to the collective modes

$$c_{m,\lambda}(k) = \frac{1}{\sqrt{N}} \sum_\alpha \mathrm{e}^{-\mathrm{i}ky_\alpha} c_\alpha(m, \lambda) \tag{3}$$

where y_α denotes the position of αth unit cell, the general states can be written by

$$|\psi(k)\rangle = \sum_{m,\lambda} \psi_{m\lambda} c^\dagger_{m,\lambda}(k)|0\rangle. \tag{4}$$

By substituting equation (4) into a Schrödinger equation with Hamiltonian (1), one can obtain the following four recurrence relations:

$$\varepsilon\psi_{mA} = \gamma_0\left(2\cos\frac{k}{2}\psi_{mB} + \psi_{m-1B}\right) + \gamma_3\left(2\cos\frac{k}{2}\psi_{m-1\tilde{B}} + \psi_{m\tilde{B}}\right) + \gamma_4\left(2\cos\frac{k}{2}\psi_{m\tilde{A}} + \psi_{m-1\tilde{A}}\right) \tag{5a}$$

$$\varepsilon\psi_{mB} = \gamma_0\left(2\cos\frac{k}{2}\psi_{mA} + \psi_{m+1A}\right) + \gamma_1\psi_{m\tilde{A}} + \gamma_4\left(2\cos\frac{k}{2}\psi_{m\tilde{B}} + \psi_{m-1\tilde{B}}\right) \tag{5b}$$

$$\varepsilon\psi_{m\tilde{A}} = \gamma_0\left(2\cos\frac{k}{2}\psi_{m\tilde{B}} + \psi_{m-1\tilde{B}}\right) + \gamma_1\psi_{mB} + \gamma_4\left(2\cos\frac{k}{2}\psi_{mA} + \psi_{m+1A}\right) \tag{5c}$$

$$\varepsilon\psi_{m\tilde{B}} = \gamma_0\left(2\cos\frac{k}{2}\psi_{m\tilde{A}} + \psi_{m+1\tilde{A}}\right) + \gamma_3\left(2\cos\frac{k}{2}\psi_{m+1A} + \psi_{mA}\right) + \gamma_4\left(2\cos\frac{k}{2}\psi_{mB} + \psi_{m+1B}\right). \tag{5d}$$

Here we use the dimensionless wavevector k in which the primitive lattice vector of the ribbon is embedded so that the range of k runs from $-\pi$ to π. Since the Z-BGNR is terminated along the x-axis, the following boundary conditions are imposed: $\psi_{0\lambda} = \psi_{N+1\lambda} = 0$. From the recurrence relations, we notice that when γ_4 is taken to be zero particle–hole symmetry exists in the band structures. In other words, for $\gamma_4 = 0$, one set of eigenvalue and eigenvector solutions of $\{\varepsilon, \psi_{mA}, \psi_{mB}, \psi_{m\tilde{A}}, \psi_{m\tilde{B}}\}$ guarantees the existence of the other orthogonal solution $\{-\varepsilon, -\psi_{mA}, \psi_{mB}, -\psi_{m\tilde{A}}, \psi_{m\tilde{B}}\}$. Hence the band structure is symmetric with respect to $\varepsilon = 0$. On the other hand, when γ_4 is included, the particle–hole symmetry is broken.

3. Electronic structure of Z-BGNRs

We study the electronic structures of Z-BGNRs with finite ribbon width N with special focus on the edge states. We first investigate a semi-infinite Z-BGNR and analytically show the signatures of the trigonal warping of the Fermi surface in the edge states. Hence our main interest lies in the bands near $\varepsilon = 0$, which contain the states localized at the ribbon edge. For $\varepsilon = 0$, the four coupled equations (5) are decomposed into the two coupled ones. One of the two coupled equations only involves ψ_B and $\psi_{\tilde{B}}$. By solving these equations, we notice that they lead to unphysical solutions unless $\psi_{mB} = \psi_{m\tilde{B}} = 0$. The other two equations, which contain ψ_A and $\psi_{\tilde{A}}$, are written as

$$\begin{aligned} &\psi_{m+2A} + \beta(2 - \bar{\gamma}_1\bar{\gamma}_3)\psi_{m+1A} + (\beta^2 - \bar{\gamma}_1\bar{\gamma}_3)\psi_{mA} = 0 \\ &\bar{\gamma}_1\psi_{m\tilde{A}} = -(\beta\psi_{mA} + \psi_{m+1A}) \end{aligned} \tag{6}$$

where $\bar{\gamma}_1 \equiv \gamma_1/\gamma_0$, $\bar{\gamma}_3 \equiv \gamma_3/\gamma_0$, and $\beta \equiv 2\cos(k/2)$. The first equation can be solved by substituting an ansatz of $\psi_{mA} \propto \mu^m$ into equation (6). As expected from the double degeneracy of band structures of bilayer graphite at the particle–hole symmetry ($\varepsilon = 0$), one can obtain two independent solutions $\mu_\pm$ as follows:

$$\mu_\pm = -\beta\left(1 - \frac{\bar{\gamma}_1\bar{\gamma}_3}{2}\right) \pm \sqrt{\bar{\gamma}_1\bar{\gamma}_3(1-\beta^2) + \beta^2\left(\frac{\bar{\gamma}_1\bar{\gamma}_3}{2}\right)^2},$$

where the localization lengths are given by $\xi_\pm = |\ln|\mu_\pm||^{-1}$.

We denote the two solutions as $\psi^\pm_{mA}$ for $\mu_\pm$ respectively. In order to have a physical normalizable solution, one needs to impose the following condition for μ: $|\mu| < 1$. This condition restricts the range of the k values supporting the zero-energy edge states as follows:

$$\text{For } \psi^+_{mA}, \qquad 2\cos^{-1}\frac{\sqrt{1+\bar{\gamma}_1\bar{\gamma}_3}}{2} \leqslant k \leqslant \pi$$

$$\text{For } \psi^-_{mA} \qquad \begin{cases} 2\cos^{-1}\dfrac{\sqrt{1+\bar{\gamma}_1\bar{\gamma}_3}}{2} \leqslant k \leqslant \dfrac{2\pi}{3} \\ 2\cos^{-1}\dfrac{1-\bar{\gamma}_1\bar{\gamma}_3}{2} \leqslant k \leqslant \pi. \end{cases} \tag{7}$$

At $k = \pi$, the edge state has the form $\psi_{mA} = (\pm\sqrt{\bar{\gamma}_1\bar{\gamma}_3})^m$ and $\psi_{m\tilde{A}} = -(\pm\sqrt{\bar{\gamma}_1\bar{\gamma}_3})^{m+1}/\bar{\gamma}_1$. Hence the localization length of a semi-infinite Z-BGNR is finite at the zone boundary, while a semi-infinite monolayer GNR is completely localized at one edge for $k = \pi$. It is interesting to notice that Z-BGNRs also support a completely localized mode at $k^* = 2\cos^{-1}\sqrt{\bar{\gamma}_1\bar{\gamma}_3}/2$ at which $\mu = 0$.

In figure 2(b), a schematic diagram of the edge states is plotted with respect to k, where the two edge modes are represented by two different colors. The yellow (pale gray) edge mode ψ^+_{mA} exists from the point T_1 at $k = 2\cos^{-1}\sqrt{1+\bar{\gamma}_1\bar{\gamma}_3}/2$ to the zone boundary, as observed in a monolayer GNR as well. Remarkably, we notice that the red (dark gray) edge mode ψ^-_{mA} has a forbidden region between the Dirac point D at $k = 2\pi/3$ and the point T_2 at $k = 2\cos^{-1}(1-\bar{\gamma}_1\bar{\gamma}_3)/2$. The existence of a forbidden region is a unique feature of Z-BGNRs. We draw two symmetric warped bands within this region, since the bands should be continuous and particle–hole symmetric. By comparing to the graphene bilayer system, the point D corresponds to the Dirac point while the points T_1 and T_2 correspond to the Fermi points of the three legs L_1, L_2 and L_3 of the graphene bilayer which are indicated in the inset of figure 2(a) [24]. This correspondence can be explicitly shown by comparing these points. A previous study of the graphene bilayer has shown that the three legs are displaced by $2\bar{\gamma}_1\bar{\gamma}_3/\sqrt{3}$ from the Dirac point D and are placed at the points with triangular symmetry [24]. If one projects these leg points onto the axis of zigzag chirality, the two leg points are located at $k = 2\pi/3 + 2\bar{\gamma}_1\bar{\gamma}_3/\sqrt{3}$ and $k = 2\pi/3 - \bar{\gamma}_1\bar{\gamma}_3/\sqrt{3}$. These values previously obtained by the $\vec{k}\cdot\vec{p}$ approximation agree perfectly with the two points T_1 and T_2 in equation (8) for small $\bar{\gamma}_1$ and $\bar{\gamma}_3$. We have confirmed the above feature of the zero-energy edge states and the warped bands by numerically solving equation (5) for relatively wide Z-BGNR with widths $N = 100$ and 200 as shown in the inset of figure 2. In order to see the above feature more clearly, we have taken values for $\bar{\gamma}_1$ and $\bar{\gamma}_3$ about five times larger than the experimental ones. Our numerical results agree well with that for a semi-infinite Z-BGNR.

Recently, Ryu *et al* suggested a criterion for the existence of edge states based on bulk energy dispersion, which may be applicable to a certain class of edge states [27]. They studied the following particle–hole symmetric Hamiltonian:

$$H = \sum_{\vec{k}} \mathbf{c}^\dagger_{\vec{k}}\mathbf{h}_{\vec{k}}\mathbf{c}_{\vec{k}} = \sum_{\vec{k}} \mathbf{c}^\dagger_{\vec{k}}\big(\vec{R}(\vec{k})\cdot\vec{\sigma}\big)\mathbf{c}_{\vec{k}} \tag{8}$$

where $\mathbf{c}^\dagger_{\vec{k}} = (c^\dagger_{\vec{k}\uparrow}, c_{\vec{k}\downarrow})$ and $\vec{\sigma}$ is a three-component vector of the Pauli matrices. This type of Hamiltonian includes the Bogoliubov–de Gennes and the GNR Hamiltonian as well. Their criterion for this Hamiltonian to have zero-energy edge sates is that the closed trajectory of $\vec{R}(\vec{k})$, being confined in a 2D plane, encloses the gap-closing point. We want to understand our result for Z-BGNRs based on the above criterion. By analyzing the 2D graphite bilayer system using the exact diagonalization method, one can obtain four energy bands, which we take to be $|\vec{R}(\vec{k})|$ [27]. We have analyzed the behaviour of one of $|\vec{R}(\vec{k})|$ s and noticed that it goes to zero three times at $k_y = 2\cos^{-1}\sqrt{1+\bar{\gamma}_1\bar{\gamma}_3}/2$, $2\pi/3$ and $2\cos^{-1}(1-\bar{\gamma}_1\bar{\gamma}_3)/2$, respectively. We presume that these three points indicate the boundaries of the three distinct topological sectors of $|\vec{R}(\vec{k})|$ where the closed loops within $2\pi/3 < k_y < 2\cos^{-1}(1-\bar{\gamma}_1\bar{\gamma}_3)/2$ exclude the gap-closing point. Hence we argue that it corresponds to the edge mode of ψ^-_{mA}. Strictly speaking, our bilayer graphene system is outside this scope, since the bilayer Hamiltonian is described by the 4×4 traceless Hermitian matrix. Furthermore, since only the magnitude of $\vec{R}(\vec{k})$ is available, we are not able to directly confirm our conjecture yet.

We now calculate the full electronic structures of Z-BGNRs with finite ribbon width N by numerically solving equation (5). We obtain the band structures of two finite width Z-BGNRs with $N = 4, 5$ as shown in figure 3. In order to study the edge states and the low-lying energy excitations analytically, we diagonalize the $4N\times4N$ matrix of equation (5) with $\varepsilon = 0$. By taking the determinant of the matrix to be zero, that is, $[(2\cos(k/2))^2 - \bar{\gamma}_1\bar{\gamma}_3]^{2N} = 0$, one can see that the band touches $\varepsilon = 0$ at $\pm k^*$ independent of N. In order to calculate the dispersion relations around $(k, \varepsilon) = (k^*, 0)$, we expand the determinant with respect to $(k^*, 0)$ and obtain the following results:

$$\varepsilon \approx \begin{cases} \pm\sqrt{\dfrac{\bar{\gamma}_1\bar{\gamma}_3}{\bar{\gamma}_1^2+\bar{\gamma}_3^2}}(2(k-k^*))^N & (N = \text{odd}) \\ \pm\sqrt{\frac{1}{2}}(2(k-k^*))^N & (N = \text{even}) \end{cases} \tag{9}$$

where ε is written in units of γ_0. These peculiar dispersions are demonstrated in our numerical result as shown in the insets of figure 3. When the ribbon width N goes to infinity, the energy dispersion becomes flattened leading to localized edge states. A similar behaviour has been observed for monolayer GNR with k^* being replaced with $k = \pi$. Unlike the monolayer GNR, a small gap opens at the zone boundary. The magnitude

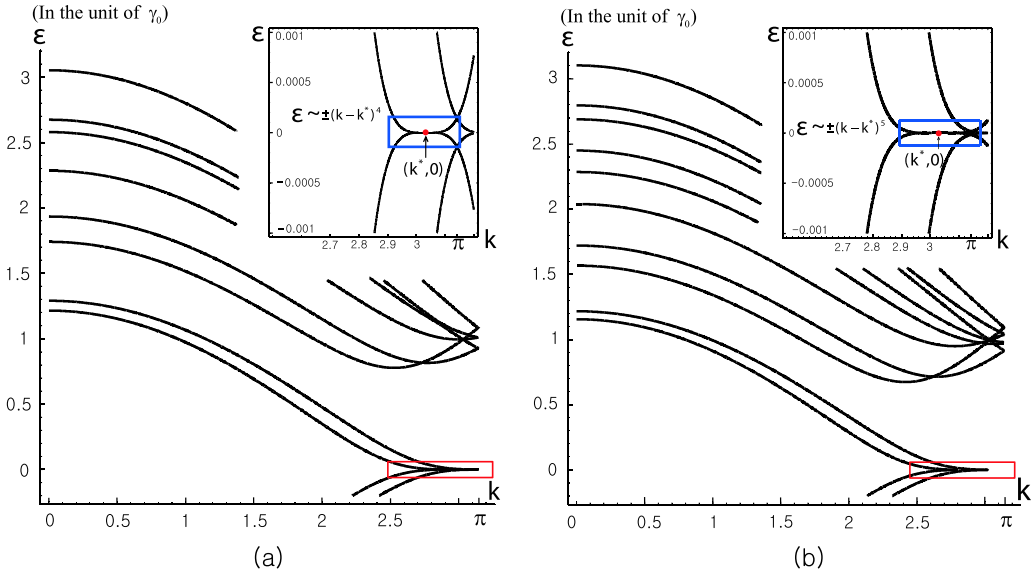

Figure 3. (a) The band diagram of a Z-BGNR with the following parameters: $\bar{\gamma}_1 = 0.12$, $\bar{\gamma}_3 = 0.1$ and $\bar{\gamma}_4 = 0$ for $N = 4$. The inset shows a magnified view of the low energy region, with power law dispersion of the edge bands. (b) The band diagram of the Z-BGNR for $N = 5$.

of the gap can be calculated approximately by considering the weak coupling between those edge modes localized at the different edges. We define the following four states which are constructed from the two semi-infinite Z-BGNRs localized at the opposite edges for $k = \pi$:

$$|L\rangle = \psi_{1A}\big(|1A\rangle - \bar{\gamma}_3|2\tilde{A}\rangle + \bar{\gamma}_1\bar{\gamma}_3|3A\rangle + \cdots\big) \tag{10a}$$

$$|\tilde{L}\rangle = \psi_{1\tilde{A}}\big(|1\tilde{A}\rangle - \bar{\gamma}_1|2A\rangle + \bar{\gamma}_1\bar{\gamma}_3|3\tilde{A}\rangle + \cdots\big) \tag{10b}$$

$$|R\rangle = \psi_{NB}\big(|NB\rangle - \bar{\gamma}_3|N-1\tilde{B}\rangle + \bar{\gamma}_1\bar{\gamma}_3|N-2B\rangle + \cdots\big) \tag{10c}$$

$$|\tilde{R}\rangle = \psi_{N\tilde{B}}\big(|1A\rangle - \bar{\gamma}_3|N-1B\rangle + \bar{\gamma}_1\bar{\gamma}_3|N-2\tilde{B}\rangle + \cdots\big), \tag{10d}$$

where $|L\rangle$ and $|\tilde{L}\rangle$ represent the localized states at the left edge, while $|R\rangle$ and $|\tilde{R}\rangle$ are those at the right edge. Using these four orthogonal states as the basis, the matrix elements of the tight binding Hamiltonian can be calculated leading to the following results:

$$\varepsilon = \begin{cases} \pm(\bar{\gamma}_1\bar{\gamma}_3)^{\frac{N}{2}} & (N = \text{even}) \\ \pm\bar{\gamma}_1(\bar{\gamma}_1\bar{\gamma}_3)^{\frac{N-1}{2}}, \pm\bar{\gamma}_3(\bar{\gamma}_1\bar{\gamma}_3)^{\frac{N-1}{2}} & (N = \text{odd}). \end{cases} \tag{11}$$

For even-width ribbons the two split edge bands in the first quadrant converge to a single value $\varepsilon = (\bar{\gamma}_1\bar{\gamma}_3)^{N/2}$ at the zone boundary, while they remain split for the odd ones. This is due to the reduced symmetry of the odd-width ribbons compared to the even ones.

According to the previous experiments, the band parameter γ_4 was assumed to be much smaller than γ_1 and γ_3 by an order of magnitude [24, 28–31]. The typical values for the hopping amplitudes are taken to be $\bar{\gamma}_1 = 0.12$, $\bar{\gamma}_3 = 0.1$ and $\bar{\gamma}_4 = 0.014$ [26]. Hence it is the usual practice to neglect the contribution of γ_4. Here we want to investigate the effect of γ_4 on the low-lying energy dispersion. Within the $\vec{k}\cdot\vec{p}$ approximation, we notice not only that the Fermi energy $\varepsilon = 0$ has a downward shift by $\Delta\varepsilon \approx -2\bar{\gamma}_1\bar{\gamma}_3^2\bar{\gamma}_4$ but also that the particle–hole symmetry is broken upon inclusion of γ_4.

Figures 4(a) and (b) show the band structures for $N = 4, 5$ obtained by numerically solving equation (5). One can observe the downward shift of the Fermi energy as expected. Interestingly, the degenerate two bands at $k = k^*$ for $\gamma_4 = 0$ are split into two bands with an indirect energy gap. We denote the extremal points as k^{e} for an electron pocket and k^{h} for a hole pocket as indicated in the insets of figure 4. When N goes to infinity, the bands become flattened.

We have closely examined the positions of k^{e} and k^{h} with increasing N and observed that the inclusion of γ_4 leads to a qualitatively different behavior. In figure 5, we plot k^{e} and k^{h} with respect to $1/N$ and extrapolate to $N \to \infty$. With increasing N, k^{e} and k^{h}, which used to be fixed at k^*, are moving toward the vicinity of the Dirac point at $k = 2\pi/3$. By fitting the energy dispersions near k_e^* and k_h^* up to $N = 4$, we find that the peculiar dispersions of $\varepsilon \sim (k - k^*)^N$ reduce to the parabolic one except for the $N = 1$ case.

4. Magnetic properties of Z-BGNRs

When the Coulomb interaction U is present in the monolayer graphene system, sublattice ferromagnetism can appear beyond a certain critical value of U. The most favorable spin configuration is known to be the opposite magnetization between two sublattices A and B, which is consistent with Lieb's theorem regarding the magnetism of bipartite lattices [32]. For the case of a zigzag GNR, the existence of almost flat bands at zero-energy stabilizes the sublattice edge ferromagnetism even for the weak Coulomb interaction. Recently it has been proposed that a zigzag GNR can become half-metallic when a transverse electric field is applied [17, 18, 22]. We have studied the edge magnetism of Z-BGNRs by applying the Hartree–Fock approximation to the

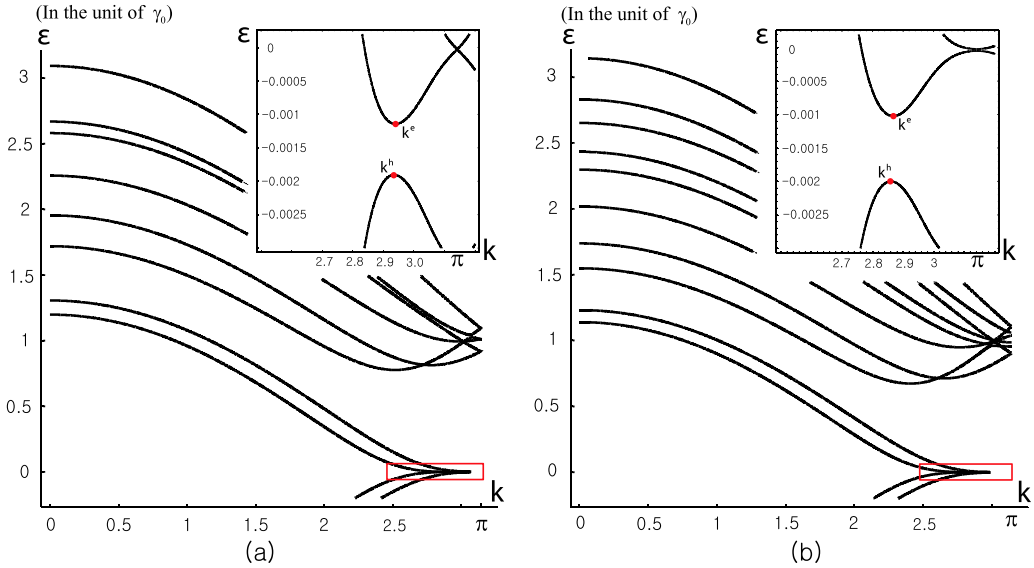

Figure 4. (a) The band diagram of the Z-BGNR with the band parameters $\bar{\gamma}_1 = 0.12$, $\bar{\gamma}_3 = 0.1$ and $\bar{\gamma}_4 = 0.014$ for $N = 4$. The inset, a magnified view of the low energy region, demonstrates broken particle–hole symmetry and parabolic dispersions. (b) The band diagram of the Z-BGNR for $N = 5$.

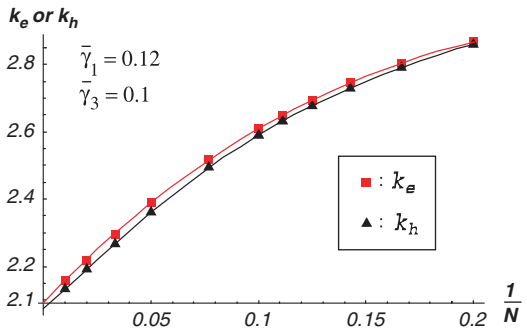

Figure 5. Plot of k^{e} and k^{h} with respect to $1/N$. The extrapolated values of k^{e} and k^{h} approach near to the Dirac point ($k = 2\pi/3 \sim 2.094$).

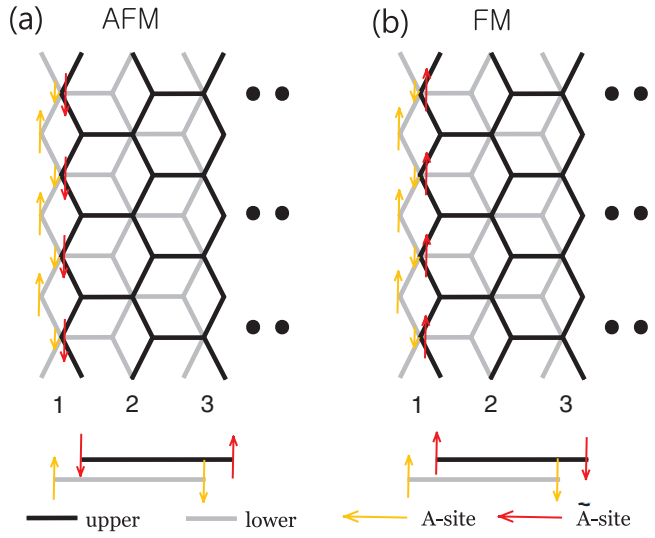

Figure 6. Two possible configurations of the magnetic moments are illustrated at the left part of the Z-BGNR. Black and gray lines represent dimer lines of the upper and lower layer, respectively. Yellow (pale gray) arrows are the magnetic moments of the lower layer while red (dark gray) arrows are for upper one. (a) The AFM configuration. At the left edge, the spin polarization at the upper ($1\tilde{A}$) and lower edge ($1A$) layer are opposite. (b) The FM configuration. The spin polarization at the upper ($1\tilde{A}$) and lower edge ($1A$) layer are parallel.

half-filled Hubbard Hamiltonian. Following the Hartree–Fock decoupling, the Hubbard Hamiltonian can be written by

$$H_{\mathrm{MF}} = -\sum_{\langle i,j\rangle,\sigma} t_{ij} c^{\dagger}_{i\sigma} c_{j\sigma} + U \sum_{i} \big[\langle n_{i\downarrow}\rangle n_{i\uparrow} + \langle n_{i\uparrow}\rangle n_{i\downarrow} - \langle n_{i\uparrow}\rangle\langle n_{i\downarrow}\rangle\big] \tag{12}$$

where we have included the on-site Coulomb interaction U and $n_{i\sigma} = c^{\dagger}_{i,\sigma} c_{i,\sigma}$. The mean electron density $\langle n_{i\sigma}\rangle$ is kept constant in a given dimer line due to translational invariance. Based on the above Hartree–Fock Hamiltonian, we have solved the self-consistent equations. Since the inter-layer hopping parameters γ_1 and γ_3 are much smaller than the intra-layer one γ_0 by an order of magnitude, we take the initial configuration for iteration as the two coupled ground state configurations of a monolayer GNR. Following the symmetry of Z-BGNRs, there exist two possible inter-layer spin configurations, as shown in figure 6. One is the anti-ferromagnetic alignment (AFM) of inter-layer edge spins within the same side of the edges: $\langle n_{A,m,\sigma}\rangle = \langle n_{\tilde{B},N-m+1,\sigma}\rangle$ and $\langle n_{B,m,\sigma}\rangle = \langle n_{\tilde{A},N-m+1,\sigma}\rangle$. The other is the ferromagnetic alignment (FM) of inter-layer edge spins: $\langle n_{A,m,\sigma}\rangle = \langle n_{\tilde{B},N-m+1,\bar{\sigma}}\rangle$ and $\langle n_{B,m,\sigma}\rangle = \langle n_{\tilde{A},N-m+1,\bar{\sigma}}\rangle$.

In order to see which configuration is energetically favorable, we have calculated the total energy of the system in those two cases. The differences between two energies $E_{\mathrm{AFM}} - E_{\mathrm{FM}}$ are plotted as a function of U in figure 7. Here we

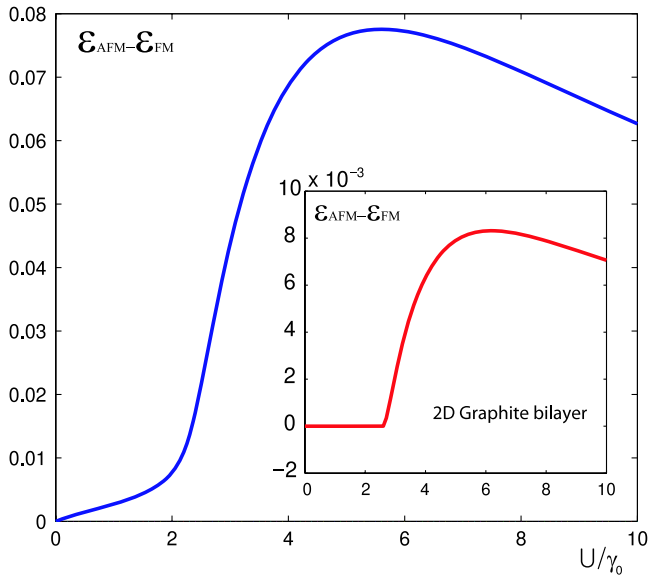

Figure 7. A plot of the energy differences per unit cell between the AFM and FM configurations for the $N = 10$ Z-BNGR and 2D graphite bilayer (inset) plotted as a function of U. The unit of energy is γ_0.

have examined a Z-BGNR of width $N = 10$ and the inter-layer hopping parameters $\bar{\gamma}_1 = \bar{\gamma}_3 = 0.1$. We notice that both AFM and FM configurations open a gap by lifting off the flat bands. Figure 7 demonstrates that the FM configuration becomes immediately stable upon including the Coulomb interaction. Since the ferromagnetic alignment of the upper and lower edge spins leads to inter-layer anti-ferromagnetic coupling between the nearest neighbor spin pairs connected by γ_1 and γ_3, the ferromagnetic alignment will become energetically favorable for large U. Hence for the experimentally relevant value of U, that is, $U/\gamma_0 \sim 1$, the FM configurations are stable [33–35]. We have also studied the bulk magnetism for the bilayer graphene system. In the inset of figure 7, the energy differences $E_{AFM} - E_{FM}$ are plotted as a function of U. With the increase of U above $U_c \cong 2.5\gamma_0$, the paramagnetic spin state becomes the FM one, which agrees with the result for the monolayer graphene system. Hence for Z-BGNRs, spin fluctuations at the edges enhance the appearance of the FM configurations even below U_c.

5. Conclusions

We have studied the electronic and magnetic structures of edge states of zigzag bilayer GNRs within the tight binding approximation. Neglecting the band parameter γ_4, we obtained a peculiar dispersion relation $\varepsilon \sim \pm(k - k^*)^N$ with $k^* = 2\cos^{-1}\sqrt{\bar{\gamma}_1\bar{\gamma}_3}/2$ which is fixed, independent of the ribbon width N. As N increases, dispersionless edge bands at $\varepsilon = 0$ appear just as for a monolayer zigzag GNR. By investigating the semi-infinite Z-BGNR analytically, we notice that trigonal warping of the graphene bilayer leads to the following interesting effect on the edge state structure of the Z-BGNR. One of the edge state at $\varepsilon = 0$ is absent within the region between the Dirac point ($k = 2\pi/3$) to $k = 2\cos^{-1}(1 - \bar{\gamma}_1\bar{\gamma}_3/2)$, where the bulk warped bands used to be present. With the inclusion of γ_4, the particle–hole symmetry is broken in our Z-BGNR system. There exists an indirect gap between two edge bands, whose band extrema are located at k^e and k^h, respectively. Instead of a fixed k^* as for the case of $\gamma_4 = 0$, k^e and k^h approach near to the Dirac point with increasing N. The magnetic properties of Z-BGNRs are studied by solving the Hubbard type Hamiltonian using the Hartree–Fock approximation. We have shown that for a realistic value of U, the ferromagnetic alignment of inter-layer edge spins within the same side of edges is favored.

Acknowledgments

We thank Y Son and J Yu for valuable discussions. This work was supported by the Korea Research Foundation Grant funded by the Korean Government (MOEHRD, Basic Research Promotion Fund) through KRF-2006-311-C00286. J Rhim acknowledges partial support from Seoul City through the program Seoul Science Scholarship. J Rhim was supported by the Brain Korea 21(BK21) project funded by the Ministry of Education and Human Resources of Korea Government.

References

[1] Han M Y, Ozyilmaz B, Zhang Y and Kim P 2007 *Phys. Rev. Lett.* **98** 206805
[2] Yang L, Park C-H, Son Y-W, Cohen M L and Louie S G 2007 *Phys. Rev. Lett.* **99** 186801
[3] Fujita M, Wakabayashi K, Nakada K and Kusakabe K 1996 *J. Phys. Soc. Japan.* **65** 1920
[4] Shyu F L, Lin M F, Chang C P, Chen R B, Shyu J S, Wang Y C and Liao c H 2001 *J. Phys. Soc. Japan* **70** 3348
[5] Miyamoto Y, Nakada K and Fujita M 1999 *Phys. Rev.* B **59** 9858
[6] Kawai T, Miyamoto Y, Sugino O and Koga Y 2000 *Phys. Rev.* B **62** 16349(R)
[7] Cancado L G, Pimenta M A, Neves B R A, Medeiros-Ribeiro G, Enoki T, Kobayashi Y, Takai K, Fukui K-I, Dresselhaus M S, Saito R and Jorio A 2004 *Phys. Rev. Lett.* **93** 047403
[8] Niimi Y, Matsui T, Kambara H, Tagami K, Tsukada M and Fukuyama H 2006 *Phys. Rev.* B **73** 085421
[9] Brey L and Fertig H A 2006 *Phys. Rev.* B **73** 235411
[10] Brey L and Fertig H A 2007 *Phys. Rev.* B **75** 125434
[11] Zheng H, Wang Z F, Luo T, Shi Q W and Chen J 2007 *Phys. Rev.* B **75** 165414
[12] Finkenstadt D, Pennington G and Mehl M J 2007 *Phys. Rev.* B **76** 121405(R)
[13] Kohmoto M and Hasegawa Y 2007 *Phys. Rev.* B **76** 205402
[14] Nakada K, Fujita M, Dresselhaus G and Dresselhaus M S 1996 *Phys. Rev.* B **54** 17954
[15] Wakabayashi K, Fujita M, Ajiki H and Sigrist M 1999 *Phys. Rev.* B **59** 8271
[16] Son Y-W, Cohen M L and Louie S G 2006 *Phys. Rev. Lett.* **97** 216803
[17] Pisani L, Chan J A, Montanari B and Harrison N M 2007 *Phys. Rev.* B **75** 064418
[18] Son Y-W, Cohen M L and Louie S G 2006 *Nature* **444** 347
[19] Klein D J 1994 *Chem. Phys. Lett.* **217** 261
[20] Fernandez-Rossier J and Palacios J J 2007 *Phys. Rev. Lett.* **99** 177204
[21] Hod O, Peralta J E and Scuseria G E 2007 *Phys. Rev.* B **76** 233401
[22] Kusakabe K and Maruyama M 2003 *Phys. Rev.* B **67** 092406

[23] Lee H, Park N, Son Y-W, Han S and Yu J 2004 *Chem. Phys. Lett.* **398** 207
Lee H, Son Y-W, Park N, Han S and Yu J 2005 *Phys. Rev.* B **72** 174431
[24] McCann E and Fal'ko V I 2006 *Phys. Rev. Lett.* **96** 086805
[25] Cserti J, Csordás A and Dávid G 2007 *Phys. Rev. Lett.* **99** 066802
[26] Charlier J-C, Gonze X and Michenaud J-P 1991 *Phys. Rev.* B **43** 4579
[27] Ryu S and Hatsugai Y 2002 *Phys. Rev. Lett.* **89** 077002
[28] Ohta T, Bostwick A, Seyller T, Horn K and Rotenberg E 2006 *Science* **313** 951
[29] Ohta T, Bostwick A, McChesney J L, Seyller T, Horn K and Rotenberg E 2007 *Phys. Rev. Lett.* **98** 206802
[30] Wang X-F and Chakraborty T 2007 *Phys. Rev.* B **75** 041404
[31] Mendez E, Misu A and Dresselhaus M S 1980 *Phys. Rev.* B **21** 827
[32] Lieb E H 1989 *Phys. Rev. Lett.* **62** 1201
[33] von Barth U and Hedin L 1972 *J. Phys. C: Solid State Phys.* **5** 1629
[34] Perdew J P, Burke K and Ernzerhof M 1996 *Phys. Rev. Lett.* **77** 3865
[35] Castro E V, Peres N and Santos J 2008 *Phys. Rev. Lett.* **100** 026802